Motion due to a moving internal heat source

By H. A. DOUGLAS, P. J. MASON

Meteorological Office, Bracknell, Berks

AND E. J. HINCH

Department of Applied Mathematics and Theoretical Physics, University of Cambridge

An experimental study has been made of the flow produced by an internal heat source as it moves around a fixed annulus of fluid. The mean surface flow relative to the annulus is found to be in the opposite direction to the movement of the heat source. The variation in its magnitude with changes in the external parameters is investigated. Thermocouple measurements and streak photography are used to examine the interior temperature and flow structure.

1. Introduction

The generation of a mean fluid motion by the passage of a propagating periodic heat source has become known as the 'moving-flame' phenomenon, after the original experiments, with a bunsen flame, by Fultz *et al.* (1959). Recent interest in the problem is due to the suggestion of Schubert & Whitehead (1969) that the phenomenon might be responsible for the 4-day circulation of Venus's atmosphere. There are also other potential applications in geophysics, to the earth's super rotation (Rishbeth 1971) and to tornadogenesis (Stern 1971). This paper is not specifically concerned with these applications, but seeks to gain insight into the phenomenon by elucidating the properties of a simple experimental (or analogue) model. In this model a moving thermal wave is created by an internal (ohmic) heat source which is made to propagate around a fixed annulus of fluid.

There have been three earlier experimental studies. The first, in which a bunsen flame was rotated beneath a cylinder of water, was by Fultz *et al.* (1959). After several minutes a steady surface flow in the opposite direction to that of the flame (i.e. a retrograde flow) with mean speeds a little less than 1 per cent of that of the flame was observed. The next study was by Stern (1959), who eliminated some of the three dimensionality present in the experiment of Fultz *et al.* by using a fixed annulus of water. Regrettably the only results reported by Stern are simply that the surface mean flows were in the opposite direction to the flame with a speed between 0·1 and 1 per cent that of the flame. More recently Schubert & Whitehead (1969) and Whitehead (1972) performed experiments similar to those of Stern, but with mercury as a working fluid. Their results are quite different from those of Stern; they found retrograde mean surface flows up to four times the speed of the flame. These large speeds give encouragement to the application of the moving-flame phenomenon to Venus, whose atmosphere

rotates approximately 25 times faster than (and in the opposite direction to) the rotation of the sun across the planet's surface.

Linear theories of the moving-flame phenomenon have been developed by Stern (1959), Davey (1967), Malkus (1970) (see Schubert, Young & Hinch 1971) and Kelly & Vreeman (1970). These theories assume that the fluid motions are small compared with the thermal wave speed. They have identified the Reynolds stress associated with the tilting of the moving convection cells as the mechanism responsible for the mean flow. This tilting may occur through thermal or viscous diffusion. (The 'knowledge' that the thermal wave is moving originates at the fixed boundaries and diffuses into the interior. There is therefore a phase lag increasing away from the boundary in any diffused quantity. This phase lag is revealed as a tilting of isotherms and streamlines.) Attempts at nonlinear theories, e.g. Hinch & Schubert (1971), have been restricted to solutions of the mean field equations in which only the fluctuating fluid velocities are assumed smaller than the thermal wave speed.

In the present experiments water was used as a working fluid and flows up to half the heat-source speed were produced. These flows are 50 times larger than those obtained by Fultz *et al.* and by Stern, and are closer to those found by Schubert & Whitehead; indeed speeds equal to those found by Schubert & Whitehead are obtained, but only in transient situations. In the boundary-heated water experiments, the heat flow into the fluid is limited by thermal boundary layers on the heated lower surface. The dynamical equivalence of internal heating and the rapid vertical heat transfer in a thin layer of mercury leads to a similarity between the present experiments and the boundary-heated mercury ones. However, Whitehead (1972) finds that the rapid flow in the mercury experiments appears to be generated by the variation of surface tension with temperature; such forces are quite negligible in the present experiments. The present experiments also differ in another important respect, namely that convective motions produce an appreciable vertical stratification.

The present experiments investigate the effect on the mean surface flow of variations in the heating rate, the thermal wave speed, the depth of the fluid layer, the cubical expansion coefficient and the viscosity. Because of the practical limitations of laboratory measurements, the present experiments necessarily lie outside the range of all the existing theories. However, the experimental results have been simplified by presentation in terms of the external dimensionless parameters. We find that the rectified flow seems to depend on the ratio of the natural convection velocity to the thermal wave speed; it is small for both small and large ratios and (at constant heating rate) is a maximum when the ratio is unity. As well as measuring the mean surface flow, the structure of the convection cells has been investigated with thermocouples and streak photographs. This development offers an insight into the mechanism which generates the mean flow; tilted isotherms and tilted convection cells are observed. The following two sections describe in detail the apparatus and the results.
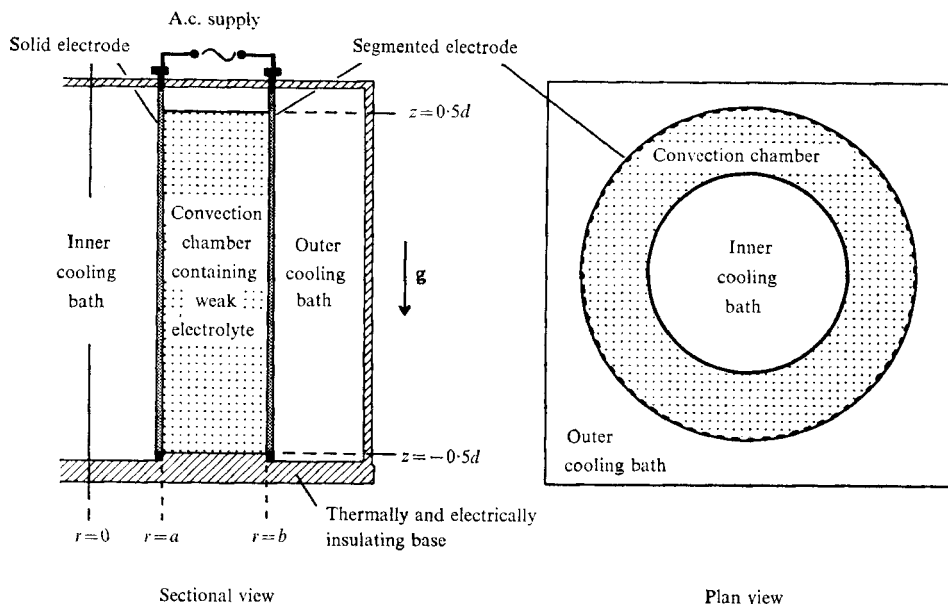
FIGURE 1. Schematic diagram of the apparatus showing the position of the two electrodes. The fluid was heated by passing an alternating current between the electrodes, and cooled by passing water through the two cooling baths. The working fluid occupies the region $a < r < b$ and $-0.5d < z < 0.5d$.

2. Apparatus

2.1. *Convection chamber*

The convection chamber (see figure 1) was the annular space of height 15 cm between two cylinders; an inner copper cylinder with radius $a = 5.0$ cm and an outer clear acrylic cylinder with radius $b = 8.5$ cm. The cylinders were secured to a horizontal electrically insulating acrylic base plate, and placed inside a clear acrylic container of square cross-section, so as to overcome a lens effect when viewing the fluid from the side. The effective bottom of the convection chamber, located at $z = -0.50d$, was the upper surface of an annular acrylic ring projecting above the level of the floors of the two cooling baths. The top of the chamber carried a flat acrylic lid above the level of the free liquid surface, eliminating effects due to evaporation and 'wind stress'. The gap width $b - a$ did not deviate from its value of 3·5 cm by more than 1 per cent as a result of unavoidable eccentricities in the shape of the bounding cylinders. The depth d was measured to an accuracy of ± 0.05 cm by means of a dipstick.

2.2. *Temperature control and internal heating*

The inner and outer cooling baths (see figure 1) were inter-connected and supplied with water circulating at about 30 cm³ s⁻¹ and kept at constant temperature to within ± 0.05 °K by means of a refrigerator and thermostat. This cooling water was passed first through the outer bath and then through the inner bath in an attempt to compensate for the lower thermal conductivity of the outer acrylic cylinder compared with that of the inner copper cylinder.

The fluid was heated internally by passing an a.c. electric current through the convection chamber. The liquid was either a weak aqueous solution of potassium sulphate or alternatively a water–glycerol solution with a trace of potassium sulphate solution added. In both cases detergent was added to reduce surface tension effects. The inner electrode was the inner copper cylinder, whereas the outer electrode consisted of 36 pairs of vertical tapes, each 0·2 cm wide and secured against the inside of the outer acrylic cylinder by annular rubber rings at the top and base of the cylinder. Each pair of tapes was connected to a micro-switch operated sequentially by a rotating cam. When viewed from the side only about a quarter of the convecting fluid, by area, was obscured by the tapes.

The rotating cam was mounted on a drive shaft connected to a synchronous induction motor via a Graham continuously variable speed transmission unit. The cam was arranged so that 9 micro-switches were always activated. As the cam moved round, the heating sector in the fluid rotated relative to the apparatus. The angular rotation rate was varied between 0 and $1 \, \mathrm{rad \, s^{-1}}$ and was accurate to better than 1 per cent over periods of the order of 1 h.

Electrical power was taken from a 50 Hz a.c. power supply with a voltage which could be varied from 0 to 300 V by means of an autotransformer. The resistance of the tapes and the inner cylinder was about 0·01 ohm and was very much less than that presented by the convecting fluid, which was about 300 ohms, so that the impressed potential differences were uniform with height. The tendency for electrical conductivity to increase with temperature (by nearly 2 per cent $°\mathrm{K^{-1}}$) was a complicating factor whose possible effects, though not serious in the experiments, have not been fully investigated. The mean voltage and current were measured by suitably calibrated dial instruments to an accuracy of ± 1 per cent for the voltage V and ± 5 per cent for the current I, giving an overall error of ± 6 per cent in the power P, which had a range of 46–$650 \, \mathrm{J \, s^{-1}}$ in the experiments. The larger uncertainty in I was a result of current fluctuations as the micro-switches were activated.

2.3. *Temperature measurements*

The temperature of the fluid in the convection chamber was measured by a thermocouple mounted in a thin steel tube, which passed through the acrylic lid in such a way as to allow the depth of the probe to be easily varied. The thermocouple was made from $2·54 \times 10^{-2}$ cm diameter copper and constantan wire, and was electrically shielded from the conducting fluid by layers of lacquer. The output from the thermocouple junction was referenced against a similar junction housed in an ice-reference unit, and the resulting output measured by a digital voltmeter. Temperature measurements were made at nominal depths of $z = -0·47d$, $-0·23d$, 0, $0·23d$ and $0·47d$, along the radius $r = \frac{1}{2}(a+b)$.

2.4. *Flow visualization*

Three different techniques of flow visualization were tried during this experiment. The results will be presented and discussed in §3; here we only present the techniques.

(i) *Dye methods.* Small crystals of dye were dropped into the annular section and the position of the resulting thin nearly vertical line noted. The new position of the leading edge of the dye line after one cycle of rotation of the heat source relative to the mean position of the line was then recorded. This technique was seldom used as, largely owing to varying rates of fall of the dye crystals, the errors were about 40 per cent; however, it was easily seen that the maximum retrograde motion occurred just below the upper surface.

(ii) *Aluminium particles.* The majority of the measurements were made by timing the movements of small aluminium flakes on the surface of the fluid. The motions were measured against a grid inscribed on the acrylic lid: the angle traversed by the particle, for one or more revolutions (relative to the particle) of the heat source, was recorded. This was taken as a measure of the Lagrangian angular velocity. For each experiment the largest angular velocities, which were found near the inner cylinder, were noted. The results were reproducible with a scatter of about 20 per cent, which was attributed to variations in surface tension. It was noticed that, on the fluid surface, motions were appreciably affected by surface tension: in the case of very weak fluid motions (weaker than those considered in §3), particles on the surface were actually stationary whilst the dye measurements beneath the surface indicated oscillating motions.

(iii) *Polystyrene beads.* A suspension of almost neutrally buoyant polystyrene beads in a water–glycerol solution was illuminated by a narrow vertical beam of light, allowing motions in a vertical plane to be studied (from the front of the apparatus). The illuminated sector was a vertical band with a radial width of 1 cm. It was curved along a constant radius in the middle $[r = \frac{1}{2}(a+b)]$ of the convection chamber and covered a sector 90° in azimuth. The flows were viewed through the flat outer wall, to reduce the lens effect due to the curvature of the cylinders.

A 35 mm camera mounted on a tripod in front of the apparatus was used to take streak photographs of the illuminated beads. A sequence of six photographs was taken, so that the position of the mid-point of the heat source was displaced by 60° between successive photographs. The centre portions of the photographs, each containing a 60° sector of the flow pattern at $r = \frac{1}{2}(a+b)$, were joined together to show the motions over a complete heating cycle. Six photographs for one cycle were considered the best compromise between curvature effects at the edges of each photograph and the number of photographs used, each photograph producing a discontinuity in the streak flow.

This method of flow visualization was found to give much information on the interior flow, but gave measures of Eulerian velocities rather than the Lagrangian velocities of the previous two methods.

2.5. *Experimental procedure*

The rotation rate of the cam switch was set to a predetermined value, the applied voltage adjusted to give the required value of P, and the cooling water set to the required temperature. The whole apparatus was allowed at least 1 h (see §3.2) to come to equilibrium before any photographs were taken or measurements made.
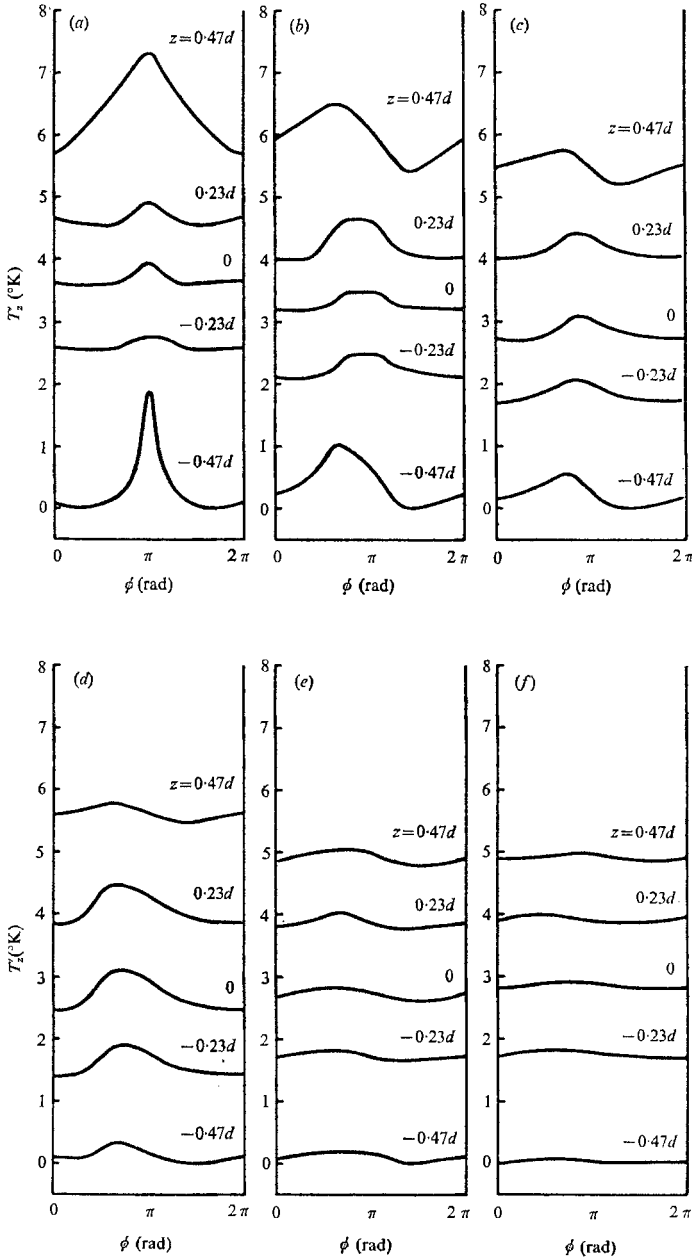
FIGURE 2. Temperature profiles for six pairs of values of ω_h, the angular speed of rotation of the heat source, and P, the power input: (a) $\omega_h = 0$, $P = 58$ J s^{-1}, (b) $\omega_h = 0.0312$ rad s^{-1}, $P = 59$ J s^{-1}, (c) $\omega_h = 0.0622$, $P = 58$, (d) $\omega_h = 0.126$, $P = 62$, (e) $\omega_h = 0.262$, $P = 54$, (f) $\omega_h = 0.523$, $P = 55$. For each set of conditions, the temperature was measured at $r = \frac{1}{2}(a+b)$ for five levels, namely $z = -0.47d$, $-0.23d$, $0d$, $0.23d$ and $0.47d$, and the plot shows the temperature difference T'_z (from the coldest point of the liquid) against the azimuthal angle ϕ measured ahead of the heat source, with origin taken so that the centre of the heat source is at $\phi = \pi$. Experimental details: liquid used was a water-glycerol solution of mean density $\bar{\rho} = 1.036$ g cm^{-3}, mean viscosity $\bar{\nu} = 1.80 \times 10^{-2}$ cm^{2}s^{-1}, mean thermal diffusivity $\bar{\kappa} = 1.26 \times 10^{-3}$ cm^2 s^{-1}, mean coefficient of cubical expansion $\bar{\alpha} = 2.33 \times 10^{-4}$ °K^{-1}; $a = 5.00$ cm, $b = 8.50$ cm, $d = 11.5$ cm.

3. Results

3.1. *Internal temperature structure*

Using the procedure described in §2.3 temperature measurements were made at five different levels in the interior of the fluid. Figure 2 illustrates the temperature profiles for each of the five levels, as functions of azimuthal angle measured ahead of the centre of the heat source. The relevant experimental details are given in the legend. Six different values of ω_h, the angular rotation speed of the heat source, were used, and owing to the variation in the mean temperature of the fluid from one experiment to the next, the zero level was arbitrarily taken as the coolest temperature of each set of profiles.

Of particular interest is the large vertical stratification set up by the convective motions; the vertical temperature differences are much larger than the azimuthal horizontal temperature differences.

When the heat source is stationary, $\omega_h = 0$, the temperature profiles are seen to be symmetric about the centre of the heated region, with particularly high temperatures at the stagnation points near the upper and lower boundaries of the fluid. When the heat source moves, the maximum temperatures are seen to occur on the trailing edge of the heat source, and the minimum temperatures on the leading edge. When the heat source moves very rapidly, e.g. $\omega_h = 0.262\,\mathrm{rad\,s^{-1}}$, and the period of rotation of the heat source becomes less than the eddy turnover time of the convective motion, the horizontal temperature contrasts in the interior of the fluid diminish.

3.2. *Surface velocity measurements*

Figure 3 is a plot of measurements of the mean retrograde Lagrangian angular velocities, ω_r, of particles of aluminium powder floating on the free surface, against the angular velocity of the heat source, ω_h. Retrograde motion is movement relative to the apparatus in the reverse sense to that of the heat source; 'prograde' motion is movement in the same sense as that of the heat source. Experimental details can be found in the legend to figure 3.

For $\omega_h = 0$, no mean flow was observed in any circumstances; any motions generated by stirring the fluid quickly decayed. For very small values of ω_h (i.e. smaller than those illustrated in figure 3) the particle motion was prograde and at the speed of the heat source. The velocities in the convective flow were much larger than the heat source velocity and a quasi-equilibrium state occurred. However, as the heat source velocity became greater than the convective velocities at the surface of the fluid, the mean motion of the aluminium particles became retrograde, with a large oscillatory component. Lagrangian mean velocities as large as 50 per cent of that of the heat source were measured. Owing to the oscillatory nature of the flow, the Eulerian mean velocities were estimated to be greater, and on occasions larger than the speed of the heat source. The diagonal line $\omega_r = \omega_h$ is shown for reference on figure 3. As ω_h is further increased, the oscillatory component of the flow decreases and the mean retrograde flow increases to a maximum. It was noted that the maximum mean flow occurred when the eddy convective velocities and the heat source velocity were approxi-
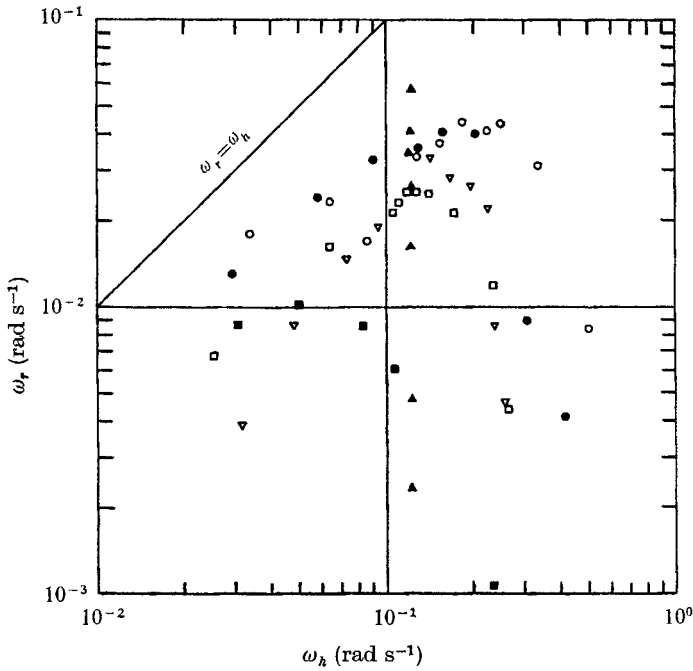
FIGURE 3. The relationship between ω_r, the angular surface rotation speed, and ω_h, the angular rotation speed of the heat source, under varying conditions.

	P (J s^{-1})	d (cm)	$\bar{\alpha}$ ($^\circ$K$^{-1} \times 10^{-4}$)	$\bar{\nu}$ (cm^2 s^{-1} $\times 10^{-2}$)	$\bar{\kappa}$ (cm^2 s^{-1} $\times 10^{-3}$)	$\bar{\rho}$ (g cm^{-3})
■†	70	11·5	2·33	1·80	1·26	1·036
□‡	162	11·5	3·21	0·77	1·46	0·995
●‡	190	11·5	4·88	0·52	1·56	0·986
○‡	510	11·5	3·90	0·66	1·49	0·992
△‡	200	3·2	4·00	0·63	1·51	0·991
	46·5	11·5	2·37	0·94	1·42	0·997
	63	11·5	2·57	0·90	1·43	0·997
	90	11·5	2·76	0·86	1·44	0·996
▲‡	163	11·5	3·21	0·77	1·46	0·995
	236	11·5	3·62	0·70	1·48	0·993
	320	11·5	4·08	0·63	1·51	0·991
	625	11·5	5·68	0·44	1·61	0·980

† Liquid used water–glycerol solution.   ‡ Liquid used water.
Other experimental details: $a = 5\cdot0$ cm, $b = 8\cdot50$ cm.

mately equal. The maximum mean surface flow was also observed to be approximately one third that of the eddy convective velocities. As ω_h is increased beyond this maximum the resultant fall-off in the mean flow is very rapid.

During the series of experiments, mean retrograde Lagrangian velocities greater than the heat source velocity were measured. These all occurred during the transition period of about 30 min, after switching on the heat source and before a final steady state was obtained. It is interesting to speculate whether these large retrograde velocities resulted from the more active convective motions present before stratification became dominant.
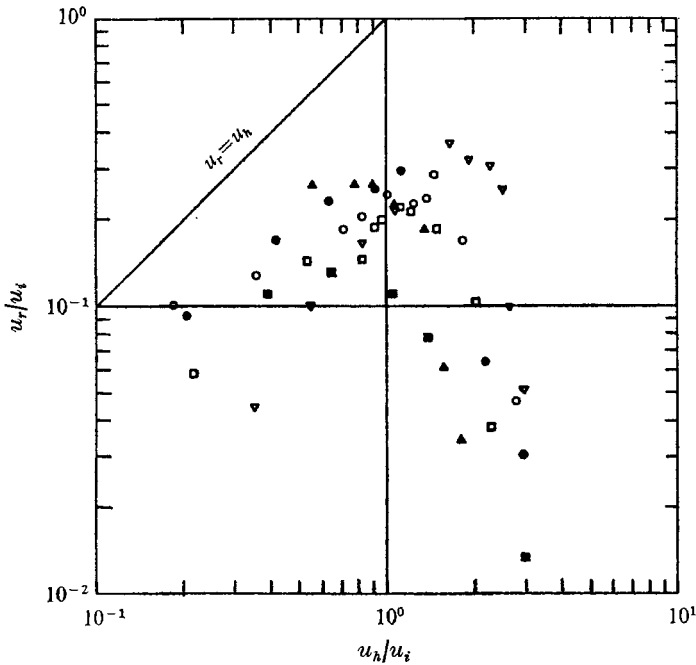
FIGURE 4. Non-dimensional plot of inertially scaled velocities for the same conditions as in figure 3. Here $u_i = [2g\overline{\alpha}Pd/\pi\overline{\rho c}(b^2-a^2)]^{\frac{1}{3}}$. The data are tending to a single curve, but a systematic shift with varying viscosity is clearly evident. See legend to figure 3 for experimental details.

This behaviour in which the retrograde motion rises to a maximum as ω_h is increased is clearly shown in figure 3 for all points for which ω_h is the only variant. The points for which only the heating power varies show a monotonic increase in the mean flow rate with the heating power. It is of interest to note that the Brunt–Väisälä frequencies are larger than any ω_h at which measurements have been made.

The observation that the maximum occurs when the heat source speed is approximately equal to the convective velocities suggests that the experimental data might be simplified by non-dimensionalization in terms of characteristic velocities of the convective motions. Without a complete theoretical solution of the convection problem we can only estimate such velocity scales crudely. Order-of-magnitude calculations based on the observed flows suggest that inertial, viscous and, for larger heat source frequencies, time-dependent effects will all be significant in determining velocities in the convective flow. However, two simple scales have been considered.

(i) An inertial velocity u_i obtained by balancing the vertical inertial and buoyancy forces in the momentum equation, the density contrast resulting from a consideration of the vertical motion of an element of fluid as it passes through the heated sector.
$$u_i = [2g\overline{\alpha}Pd/\pi\overline{\rho c}(b^2-a^2)]^{\frac{1}{3}}.$$

(ii) Similarly, by balancing vertical components of viscous and buoyancy forces we have
$$u_v = [g\overline{\alpha}P(b-a)/12\pi\overline{\rho c}\overline{\nu}(b+a)]^{\frac{1}{2}}.$$
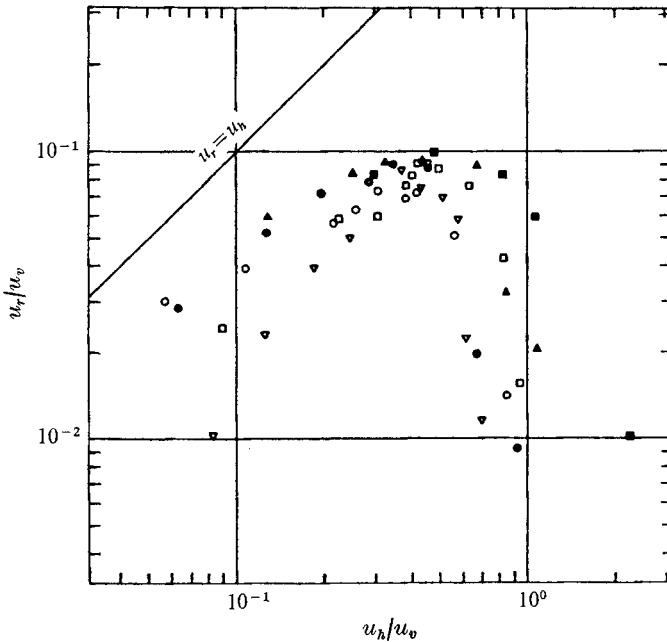
FIGURE 5. Non-dimensional plot of viscously scaled velocities for the same conditions as in figures 3 and 4. Here

$$u_v = [g\bar{\alpha}P(b-a)/12\pi\bar{\rho}\bar{c}\bar{\nu}(b+a)]^{\frac{1}{2}}.$$

The data are closer to a single curve than in figure 4, but there is still a systematic shift of data. See legend to figure 3 for experimental details.

(g is the accleration due to gravity, $\bar{\alpha}$ is the mean coefficient of cubical expansion, $\bar{\rho}$ the mean density of the fluid, $\bar{\nu}$ the mean viscosity and $\bar{c}$ the mean specific heat.)

The appropriate length and aspect ratio values to use in these scale velocities are not obvious, especially in the viscous case. An arbitrary choice has been made which, whilst affecting the size of the non-dimensional velocities, does not affect the degree to which the data are simplified.

The non-dimensional plot of inertial scale velocities is shown in figure 4. The mean deviation from a single curve is ± 43 per cent, cf. ± 170 per cent in figure 3, but a systematic shift with varying viscosity is clear from the graph.

The non-dimensional plot of viscous scale velocities (figure 5) gives a better sorting on to a single curve (except for large ω_h). The mean deviation from a single curve is ± 29 per cent, which compares favourably with the typical experimental errors of ± 15 per cent.

The degree of fitting of the data onto a single curve using only crude scale velocities is promising and seems to confirm the experimental observation that the resultant rectified flow is determined by the ratio of the interior convection velocities to the velocity of the heat source. The rise to the maximum at smaller values of u_h/u_i or u_h/u_v has a slope of about one. The fall-off from the maximum at higher values of u_h/u_i or u_h/u_v is very rapid. However, when scale velocities based on time-dependent effects are considered, the magnitude of the slope of

this rapid fall-off is reduced to about one. The time-dependent scale velocity plots are not presented here for, with the exception of the measurements at high heat source frequencies, the degree of fitting of the data onto a single curve is less than with the inertial and viscous scale velocities.

3.3. *Interior flow structure*

These final experimental results in which the interior flow patterns are presented will be of particular interest in any theoretical understanding of the rectification process. Figure 6 (plate 1) shows a series of composite photographs, taken using the method described in §2.4, for five different values of ω_h corresponding to the first five temperature profiles shown in figure 2.

When the heat source is stationary, the flow is symmetric about the centre of the heat source, with boundary layers on the top and bottom of the convecting fluid and a strong upwelling within the heated region. The downward return flow is accomplished outside the photographed segment of the fluid, in boundary layers on the inner and outer cylinders.

With the heat source moving slowly (i.e. ω_h less than the value for maximum rectification) the flow is typically as shown in figure 6 (b) (here $\omega_h = 0.0312\,\mathrm{rad\,s^{-1}}$). The flow is no longer symmetric about the centre of the heat source but in the lower boundary layer there is a stronger inflow upstream of the heat source, and in the upper surface boundary layer there is a stronger outflow downstream. The free-surface velocities show a mean retrograde motion for these values of ω_h.

When the heat source is moved faster than the speed required for maximum rectified flow, the flow is typically as shown in figure 6 (d) (here $\omega_h = 0.126\,\mathrm{rad\,s^{-1}}$). The centre of the upwelling motion appears appreciably downstream of the heat source. The pronounced backward tilt of the convection cell clearly indicates rectified flow. Some downward motion is now occurring in the body of the fluid as well as in the boundary layers on the inner and outer cylinders.

When the heat source moves at the speed for maximum rectification (figure 6 (c): $\omega_h = 0.062\,\mathrm{rad\,s^{-1}}$) the flow is complex, exhibiting features common to the surrounding photographs in figures 6 (b) and (d).

When the heat source moves at the fastest speeds used in the photographs ($\omega_h = 0.262\,\mathrm{rad\,s^{-1}}$), the motion in the interior appears to be very weak and is rising everywhere with a slight retrograde mean. The return flow is again out of the picture, in the outer and inner wall boundary layers.

REFERENCES

DAVEY, A. 1967 *J. Fluid Mech.* **29**, 137.

FULTZ, D., LONG, R. R., OWENS, G. V., BOHAN, W., KAYLOR, R. & WEIL, J. 1959 *Met. Monograph*, **4** (21), 36.

HINCH, E. J. & SCHUBERT, G. 1971 *J. Fluid Mech.* **47**, 291.

KELLY, R. E. & VREEMAN, J. D. 1970 *Z. angew. Math. Phys.* **21**, 1.

MALKUS, W. V. R. 1970 *J. Atmos. Sci.* **27**, 529.

RISHBETH, H. 1971 *Nature*, **229**, 333.

SCHUBERT, G. & WHITEHEAD, J. A. 1969 *Science*, **163**, 71.

SCHUBERT, G., YOUNG, R. E. & HINCH, E. J. 1971 *J. Geophys. Res.* **76**, 2126.

STERN, M. E. 1959 *Tellus*, **11**, 175.

STERN, M. E. 1971 *Tellus*, **23**, 122.
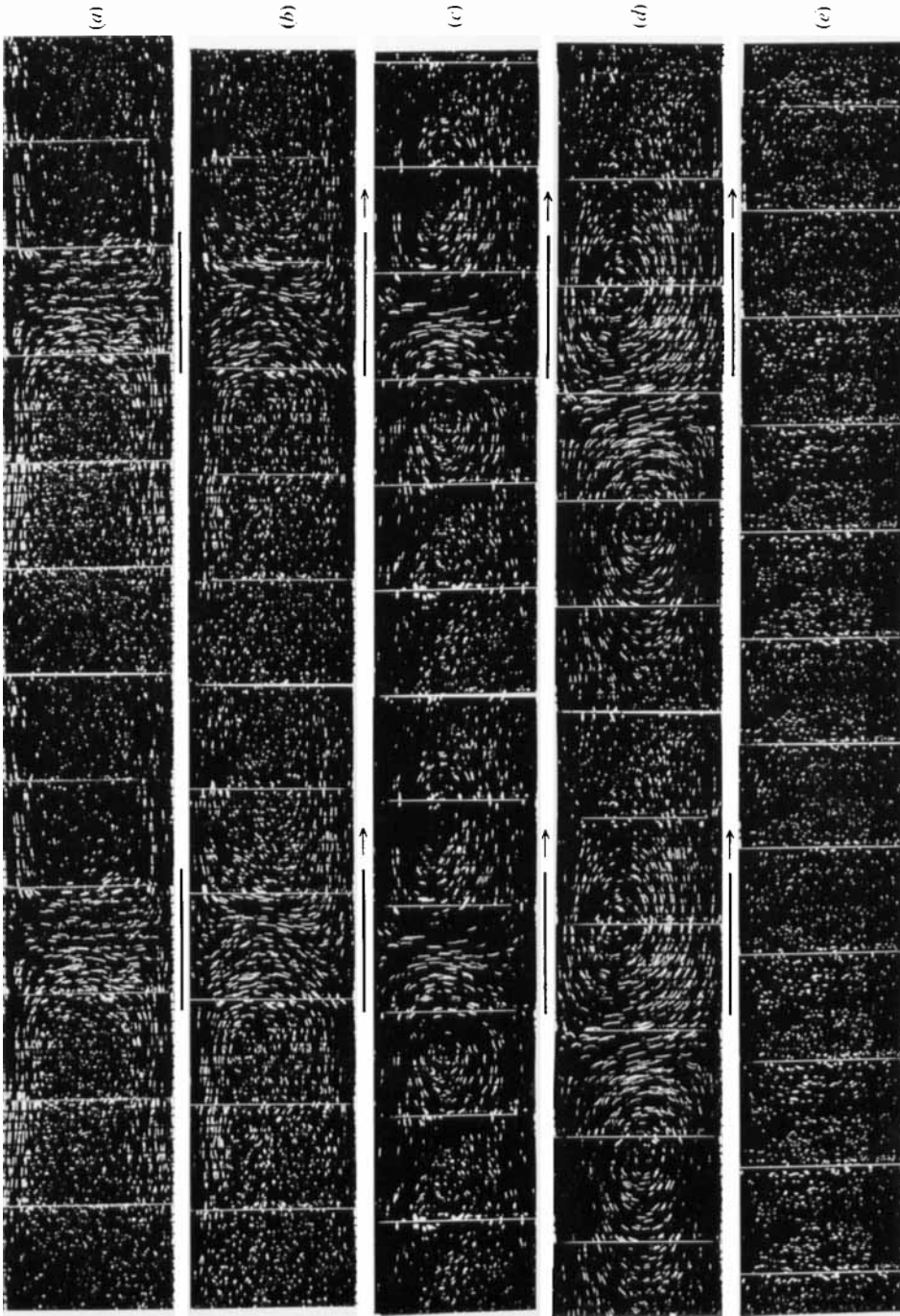
WHITEHEAD, J. A. 1972 *Geophys. Fluid Dyn.* **3**, 161.

FIGURE 6. The internal flow structure in a vertical plane, through two heating cycles, for each of five values of ω_h, the angular speed of rotation of the heat source. In each case, the solid bar denotes the sector which is being internally heated, and the arrows show the sense of movement of this heated region. (a) $\omega_h = 0$, exposure time $\tau = 6$ s; (b) $\omega_h = 0.0312$ rad s^{-1}, $\tau = 5$ s; (c) $\omega_h = 0.0622$, $\tau = 5$; (d) $\omega_h = 0.126$, $\tau = 5$; (e) $\omega_h = 0.262$, $\tau = 3$. Experimental details: liquid used was a water–glycerol solution of mean density $\bar{\rho} = 1.036$ g cm^{-3}; $\bar{\nu} = 1.80 \times 10^{-2}$ cm^2 s^{-1}, $\bar{\kappa} = 1.26 \times 10^{-3}$ cm^2 s^{-1}, $\bar{\alpha} = 2.33 \times 10^{-4}$ $^{\circ}$K^{-1}, $P = 56 \pm 2$ J s^{-1}.